Available online at www.sciencedirect.com
ScienceDirect
Nuclear Engineering and Design 238 (2008) 1947–1957
Nuclear Engineering and Design
www.elsevier.com/locate/nucengdes

Numerical analysis of supercritical flow instabilities in a natural circulation loop

Prashant K. Jain *, Rizwan-uddin

Department of Nuclear, Plasma and Radiological Engineering, University of Illinois at Urbana-Champaign, 216 Talbot Lab, 104 S. Wright Street, Urbana, IL 61801, USA

Received 20 March 2007; received in revised form 16 October 2007; accepted 16 October 2007

Abstract

Numerical studies have been carried out to investigate flow instabilities in a natural circulation loop with supercritical CO_2. For steady-state and dynamic analyses of the loop under supercritical conditions, a single-channel, one-dimensional model is developed. In this model, equations for the conservation of mass, momentum and energy are discretized using an implicit finite difference scheme. A computer code called *f*low *i*nstability *a*nalysis under *s*uper*c*ritical *o*perating conditions (FIASCO) is written in FORTRAN90 to simulate the dynamics of natural circulation loops with supercritical fluid. Stability boundaries are determined by simulating the loop's time evolution following a small perturbation under different operating conditions. Stability threshold results substantially deviate from the results reported by previous investigators, and contradict some of the reported findings. The disagreement in results is most likely due to the undesirable dissipative and dispersive effects produced from the large time steps used in previous studies, thereby leading to a larger stable region than those found using smaller time steps. Results presented in this paper suggest that the stability threshold of a natural circulation loop with supercritical fluid is not confined to the *near-peak region* of the (steady state) flow-power curve. Results obtained for the range of parameter values used in this investigation always predict the stability threshold to be in the positive slope region of the (steady state) flow-power curve. Parametric studies for different operating conditions reveal the similarity of stability characteristics of flow under supercritical conditions with those in two-phase flows.

1. Introduction

Supercritical water-cooled reactor (SCWR) is one of the advanced nuclear reactor systems selected under the Generation IV program for cost-effective energy generation, and safety. The SCWR concept, which evolved from the Japanese supercritical light water reactor (SCLWR), has a thermal neutron spectrum, and is cooled and moderated by supercritical light water (GIF, 2002; Buongiorno, 2004). This reactor system may have potential to improve fuel economy and may simplify plant design considerably. Moreover, compared with the LWRs, higher thermal efficiency and lower coolant mass flow rate *per unit core thermal power* can be achieved with SCWRs (Yamaji et al., 2005). The design is also rated "good" in the categories of safety, proliferation resistance and physical protection. This is due to its passive safety features which are designed to avoid accidents and reduce operator dependability (GIF, 2002).

SCWR design is built upon two well-developed technologies: light water reactors (LWRs) and supercritical fossil-fired boilers. In SCWR, operation at supercritical pressure (25.0 MPa) eliminates coolant boiling, so the coolant always remains in single-phase throughout the system; and superheated steam can be obtained without the danger of dryout in the core. However, a gradual deterioration in heat transfer may occur in the *near-critical region* (narrow region around the pseudo-critical point), but does not result in significant drop in the heat transfer coefficients to values associated with dryout (Pioro et al., 2004). Additionally, employment of single-loop cycle in which coolant directly circulates to and fro from the core to the turbine remarkably simplifies the nuclear system eliminating the need of recirculation lines, pressurizer, steam separators and dryers. In short, SCWR design takes advantage of the desirable feature of BWR over PWR (single loop) without the associated disadvantage (boiling). Moreover, the mass flow rate of coolant in

* Corresponding author. Tel.: +1 217 244 7600; fax: +1 217 333 2906.
E-mail address: pkjain2@uiuc.edu (P.K. Jain).

0029-5493/$ – see front matter © 2008 Elsevier B.V. All rights reserved.
doi:10.1016/j.nucengdes.2007.10.034

Nomenclature

C_k	coefficient in momentum conservation equation
D_h	hydraulic diameter (m)
f	friction coefficient
g	acceleration due to gravity (m/s^2)
h	specific enthalpy (J/kg)
i	grid index
m	index for the last grid point
n	time step index
p	pressure (N/m^2)
q'''	volumetric heat addition rate (W/m^3)
R_{k_1}	inlet restriction coefficient
R_{k_2}	exit restriction coefficient
Re	Reynolds number
t	time (s)
Δt	time step size (s)
u	velocity (m/s)
z	axial distance (m)
Δz	spatial grid size (m)

Greek symbols

η	$=\Delta z/2\Delta t$
θ	angle of flow direction with respect to horizontal plane (rad)
ρ	density (kg/m^3)
μ	dynamic viscosity (N s/m^2)

SCWR is low, and core exit temperature is high with a large temperature increase across the core, thereby resulting in a high plant thermal efficiency of about 44% (Yamaji et al., 2005).

Due to supercritical operating conditions in SCWR, thermodynamic and transport properties of water change significantly as its temperature approaches the pseudo-critical point, where the distinction between liquid and vapor phases disappears. The thermal conductivity and the heat capacity at constant pressure tend to increase dramatically, while the thermal diffusivity tends to zero (Zappoli, 2003). Also, density and viscosity tend to decrease significantly as fluid temperature approaches the pseudo-critical point. Some of these changes are similar in magnitude to those encountered during boiling with phase change. [It may be noted that there is no phase transition (i.e. no two phase) of water as its temperature crosses the pseudo-critical point.]

Similar to BWRs, SCWR core will experience large changes in density across the core and therefore may be susceptible to flow instabilities similar to those observed in BWRs (such as density-wave instabilities, and coupled neutronic–thermohydraulic instabilities). Thermal hydraulic instabilities resulting in flow oscillations will be highly undesirable in SCWR system, as they may: (1) give rise to nuclear instabilities (due to density-reactivity feedback); (2) result in failure of control mechanism; or (3) lead to fatigue damage of reactor components. Therefore, the licensing of SCWR will require demonstrable capability to predict the onset of instabilities. Consequently, it is necessary to understand the instability phenomena in SCWR and identify the variables which affect these phenomena. The ultimate goal of a stability analysis is to generate stability maps to identify stable operating conditions for SCWR design (Yang and Zavaljevski, 2003, 2004). Moreover, emphasis in SCWR design is also placed on passive safety mechanisms by employing, for example, natural circulation cooling systems (rather than forced ones) to remove core decay heat after accidental reactor shutdown. Consequently, it is necessary to study SCWR stability under forced as well as natural circulation conditions.

The natural circulation loop with supercritical flow conditions – similar to a corresponding forced circulation system – experiences a rather large density change across a very small temperature range near the pseudo-critical point. This may lead the system towards instabilities similar to those observed in heated channels with two-phase flows. Instabilities in natural circulation loops with supercritical flow, associated with the two-phase-like property variation of single-phase supercritical fluid, near the pseudo-critical point have not been fully explored. Hence, a study of flow stability phenomena in a natural circulation loop with supercritical fluid is carried out in this paper. This study can easily be extended, by introducing a neutronics model, to analyze SCWR instabilities, i.e. coupled neutronic–thermohydraulic instabilities, as well. Recent work on stability of supercritical fluid flow in a single-channel, natural-convection loop is reviewed below.

A model of supercritical flow to study system stability of a simplified single-channel, natural-convection configuration is developed by Chatoorgoon (1986, 2001). The configuration is a constant cross-section area loop with constant boundary conditions for inlet temperature, inlet pressure and outlet pressure. The same point source and point sink configuration is also simulated using the special predictions of reactor transients and stability (SPORTS) code, and good agreement is reported in bounding power for stable flows. Chatoorgoon also studied the supercritical flow stability phenomenon numerically in the same loop with distributed heat source and sink, using the SPORTS code. More recently, Chatoorgoon and Upadhye (2005) and Chatoorgoon et al. (2005a,b) reported extended analytical and numerical studies examining the effects of several different parameters on supercritical flow stability including inlet temperatures, inlet and outlet channel restriction coefficients (K factors), different loop heights and heated lengths. In addition, these studies also included effect of different fluids like CO_2 and H_2O. Based on the numerical results obtained it is concluded that stability characteristics of supercritical CO_2 are very similar to that of supercritical H_2O. Very recently, stability analysis in a uniformly heated channel (Gomez et al., 2006; Ambrosini and Sharabi, 2006) as well as in parallel channel (Chatoorgoon et al., 2007) with supercritical fluid has been reported.

There have been very few experimental studies of natural circulation with fluids near the critical point. Recently, experimental results of a natural circulation supercritical water (SCW) loop have been reported (Lomperski et al., 2004). Also, experimental data have been reported for flow in a rectangular test loop with CO_2. Operation with CO_2, instead of water, allows

operation at moderate temperature and pressure (Jain, 2005). These experimentally obtained stability thresholds deviate significantly from numerical predictions made by Chatoorgoon et al. (2005b) and Jain (2005).

2. Model

Flow stability is usually studied by solving the time-dependent mass, momentum and energy conservation equations representing the system. These equations are generally solved either in frequency-domain or time-domain to determine stability boundaries in appropriate parameter spaces.

In the frequency-domain approach, the conservation equations along with the necessary constitutive laws are linearized about an operating point and Laplace transformed. Stability predictions are then made by applying such well-known methods as Bode plot, Nyquist plot, root-locus techniques, etc. Though very valuable, results of these frequency domain approaches are valid for infinitesimal perturbations only.

In the time-domain approach, the conservation equations are solved numerically using, for example, finite-difference techniques. Usually, this approach is very time consuming when used for stability analyses, since the allowable time step size may be very small, and large numbers of cases must be run to generate a stability map. However, with ever increasing computational resources, time domain stability analysis is becoming more prevalent. It is usually performed to predict the threshold value of a system parameter (for example, heat flux or power level) below (or above) which the system is stable. Usually, the set of steady-state equations are solved first. The steady-state solution, with a perturbation, is then used as the initial condition for the transient flow. The perturbation can either be a fractional change in the steady-state solution or a small change in one or more system parameters (like heat flux, pressure drop coefficient, etc.) that lasts a short period of time. System stability can also be investigated by momentarily perturbing the boundary condition(s). If the disturbance grows in time and yields sustained or diverging flow oscillations, then the steady-state system is considered to be unstable. On the other hand, if the disturbance leads to decaying oscillations resulting in convergence of flow and other field variables to the steady-state solution, then the corresponding steady-state solution is considered to be stable.

Steady-state and dynamic analyses of supercritical water loop (SCWL) require appropriate modeling of the thermodynamic and transport properties of the working fluid near its critical point. Due to high non-linearities associated, multi-dimensional modeling of the coolant channel becomes too complex. Therefore, for this preliminary investigation, a single-channel, one-dimensional model is developed (Jain and Rizwan-uddin, 2006). In this model, equations for the conservation of mass, momentum and energy are discretized using an implicit finite difference scheme. Details of the model are described below.

2.1. Steady-state equations

For one-dimensional channel flow, the steady-state mass, momentum and energy conservation equations, and the equation of state can be written as follows:

Continuity:

$$\frac{\partial(\rho_{ss}\, u_{ss})}{\partial z} = 0 \tag{1}$$

Momentum conservation:

$$\frac{\partial(\rho_{ss}\, u_{ss}^2)}{\partial z} + \frac{\partial p_{ss}}{\partial z} + C_k\, \rho_{ss}\, u_{ss}^2 + \rho_{ss}\, g\, \sin\theta = 0 \tag{2}$$

Energy conservation:

$$\frac{\partial}{\partial z}\left[\rho_{ss}\, u_{ss}\left(h_{ss} + \frac{u_{ss}^2}{2}\right)\right] + \rho_{ss}\, u_{ss} g \sin\theta = q''' \tag{3}$$

State:

$$\rho_{ss} = \mathrm{eos}(p_{ss}, h_{ss}) \tag{4}$$

where ρ_{ss}, u_{ss}, p_{ss} and h_{ss} are the fluid density, velocity, pressure and enthalpy, respectively, at steady-state conditions. Also, g is the acceleration due to gravity, θ the angle of the flow direction from the horizontal plane (anti-clockwise), and q''' is the volumetric heat generation rate. Also, eos represents equation of state.

Coefficient C_k in the momentum conservation equation (Eq. (2)) is given by

$$C_k = \frac{f_{ss}}{2D_h} \tag{5}$$

where D_h is the hydraulic diameter of the channel and f_{ss} is the friction factor, which can be determined using the Blasius and McAdams relations (McAdams, 1954) for a smooth tube, given by

$$f_{ss} = \begin{cases} 0.316\, Re_{ss}^{-0.25}, & Re_{ss} < 30,000 \\ 0.184\, Re_{ss}^{-0.20}, & 30,000 < Re_{ss} < 10^6 \end{cases} \tag{6}$$

Here Re_{ss} is the Reynolds number defined as

$$Re_{ss} = \frac{\rho_{ss}\, u_{ss}\, D_h}{\mu_{ss}} \tag{7}$$

and μ_{ss} is the dynamic viscosity [ss in subscript represents steady-state conditions].

2.2. Time-dependent equations

For one-dimensional channel flow, the time-dependent mass, momentum and energy conservation equations, and the equation of state can be written as follows:

Continuity:

$$\frac{\partial \rho}{\partial t} + \frac{\partial(\rho u)}{\partial z} = 0 \tag{8}$$

Momentum conservation:

$$\frac{\partial(\rho\, u)}{\partial t} + \frac{\partial(\rho\, u^2)}{\partial z} + \frac{\partial p}{\partial z} + C_k\, \rho\, u^2 + \rho\, g\, \sin\theta = 0 \tag{9}$$

Energy conservation:

$$\frac{\partial}{\partial t}\left[\rho\left(h+\frac{u^2}{2}\right)\right]+\frac{\partial}{\partial z}\left[\rho u\left(h+\frac{u^2}{2}\right)\right]+\rho u g\sin\theta = \frac{\partial p}{\partial t}+q''' \tag{10}$$

State:

$$\rho = \mathrm{eos}(p,h) \tag{11}$$

where ρ, u, p and h are the fluid density, velocity, pressure and enthalpy, respectively. Other definitions are the same as those given at the end of Section 2.1.

The set of mass, momentum and energy conservation equations is closed by the equation of state for the supercritical fluid. In this study, supercritical properties of water and CO_2 are determined by employing NIST/STEAM 2.21 (Harvey et al., 2004) and NIST/REFPROP7 (Lemmon et al., 2002), respectively.

3. Numerical approach

The governing equations, which form a system of non-linear equations, are solved numerically. Control-volume-based discretization in space and forward-difference scheme in time are employed to derive the difference equations for the mass, momentum and energy conservation.

The one-dimensional flow channel is divided into axial computational cells or control volumes, with the grid points located at the cell edges as shown in Fig. 1. The first and last grid points of the domain coincide with the flow channel physical boundaries.

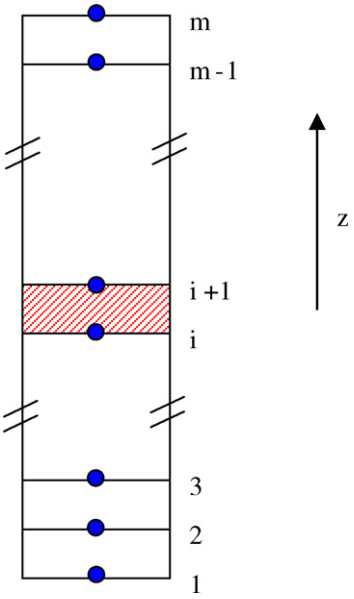

Fig. 1. Spatial grid and control volume in the flow channel.

3.1. Discretized equations for the steady-state problem

Integration of the steady-state conservation equations (Eqs. (1)–(4)) from grid point (i) to ($i+1$) leads to the following set of discretized equations:

Continuity:

$$(u_{ss})_{i+1} = \frac{(\rho_{ss}\,u_{ss})_i}{(\rho_{ss})_{i+1}} \tag{12}$$

Momentum conservation:

$$(p_{ss})_{i+1} = (p_{ss})_i - \left(1+\frac{1}{2}(C_k)_{i+1}\,\Delta z\right)(\rho_{ss}\,u_{ss}^2)_{i+1} + \left(1-\frac{1}{2}(C_k)_i\,\Delta z\right)(\rho_{ss}\,u_{ss}^2)_i - \left(\frac{(\rho_{ss})_i+(\rho_{ss})_{i+1}}{2}\right) g\,\Delta z\sin\theta_i \tag{13}$$

Energy conservation:

$$(h_{ss})_{i+1} = \frac{(q_i'''+q_{i+1}'''/2)\,\Delta z - ((\rho_{ss}\,u_{ss})_{i+1}+(\rho_{ss}\,u_{ss})_i/2)\,g\,\Delta z\sin\theta_i + (\rho_{ss}\,u_{ss}\,h_{ss})_i}{(\rho_{ss}\,u_{ss})_{i+1}} \tag{14}$$

State:

$$(\rho_{ss})_{i+1} = \mathrm{eos}((p_{ss})_{i+1},(h_{ss})_{i+1}) \tag{15}$$

where the friction coefficient $(C_k)_i$ in Eq. (13) is defined by

$$(C_k)_i = \frac{f_{ss,i}}{2D_h} = \frac{1}{2D_h}\begin{cases} 0.316(\mathrm{Re}_{ss}^{-0.25})_i, & \mathrm{Re}_{ss,i} < 30,000 \\ 0.184(\mathrm{Re}_{ss}^{-0.20})_i, & 30,000 < \mathrm{Re}_{ss,i} < 10^6 \end{cases} \tag{16}$$

Here $\mathrm{Re}_{ss,i}$ is given by

$$\mathrm{Re}_{ss,i} = \frac{(\rho_{ss}\,u_{ss})_i}{\mu_{ss,i}}D_h \tag{17}$$

3.2. Discretized equations for the time-dependent problem

Integration of the time-dependent conservation equations (Eqs. (8)–(11)) from grid point (i) to ($i+1$) and forward-difference approximation for the time derivative yield the following set of implicit discretized equations:

Continuity:

$$u_{i+1}^{n+1} = \frac{(\rho u)_i^{n+1} - \eta(\rho_i^{n+1}-\rho_i^n+\rho_{i+1}^{n+1}-\rho_{i+1}^n)}{\rho_{i+1}^{n+1}} \tag{18}$$

Momentum conservation:

$$p_{i+1}^{n+1} = p_i^{n+1} - \left(1+\frac{1}{2}(C_k)_{i+1}^n\,\Delta z\right)(\rho u^2)_{i+1}^n + \left(1-\frac{1}{2}(C_k)_i^n\,\Delta z\right)(\rho u^2)_i^n - \left(\frac{\rho_i^n+\rho_{i+1}^n}{2}\right) g\,\Delta z\sin\theta_i + \eta((\rho u)_i^{n+1}-(\rho u)_i^n+(\rho u)_{i+1}^{n+1}-(\rho u)_{i+1}^n) \tag{19}$$

Energy conservation:

$$h_{i+1}^{n+1} = \frac{(q_i''' + q_{i+1}'''/2)\,\Delta z - ((\rho u)_{i+1}^{n+1} + (\rho u)_i^{n+1}/2)\,g\,\Delta z \sin\theta_i - \eta\{(\rho h)_i^{n+1} - (\rho h)_{i+1}^n - (\rho h)_i^n\} + (\rho u h)_i^{n+1}}{(\rho u)_{i+1}^{n+1} + \eta\,\rho_{i+1}^{n+1}} \quad (20)$$

State:

$$\rho_{i+1}^{n+1} = \mathrm{eos}(p_{i+1}^{n+1}, h_{i+1}^{n+1}) \quad (21)$$

where the friction coefficient $(C_k)_i^n$ in Eq. (19) is defined by

$$(C_k)_i^n = \frac{f_i^n}{2D_\mathrm{h}} = \frac{1}{2D_\mathrm{h}} \begin{cases} 0.316(\mathrm{Re}^{-0.25})_i^n, & \mathrm{Re}_i^n < 30,000 \\ 0.184(\mathrm{Re}^{-0.20})_i^n, & 30,000 < \mathrm{Re}_i^n < 10^6 \end{cases} \quad (22)$$

and Re_i^n is given by

$$\mathrm{Re}_i^n = \frac{(\rho u)_i^n}{\mu_i^n} D_\mathrm{h} \quad (23)$$

In the above set of discrete equations, η is given by $\Delta z/2\Delta t$ where Δz and Δt correspond to the spatial grid size and time step, respectively.

In deriving the difference equations, the effect of integrating across a computational cell is analogous to averaging the field and flow variables in that cell, and leads to better accuracy compared to the first-order difference scheme for the spatial derivatives.

3.3. Boundary conditions

Solution of the system of non-linear governing equations depends upon the choice of boundary conditions. For the present investigation, constant pressure drop boundary condition along with constant inlet conditions are applied to the flow channel, i.e. inlet temperature, inlet pressure and outlet pressure are assumed to be prescribed.

For the case of zero total pressure drop inside the flow channel (natural circulation), these boundary conditions may be physically achieved by connecting both ends of the channel to a large reservoir, in which pressure and temperature are maintained at constant values (Chatoorgoon, 2001; Chatoorgoon et al., 2005a,b; Jain, 2005).

3.4. Solution algorithm

3.4.1. Solution algorithm for the steady-state problem

The algorithm employed to solve the coupled, non-linear, steady-state equations (Eqs. (12)–(15)) is given below (Chatoorgoon, 1986):

There are four unknown variables (ρ_{ss}, u_{ss}, p_{ss} and h_{ss}) to be solved for each grid point i.

(1) Inlet conditions of the flow channel are maintained constant, therefore, at grid point 1:
- $(\rho_{ss})_1 = \rho_{in} =$ constant.
- $(p_{ss})_1 = p_{in} =$ constant.
- $(h_{ss})_1 = h_{in} =$ constant.

(2) Velocity at the channel inlet $(u_{ss})_1$ is guessed.

(3) Steps (a) and (b) below are repeated for $i = 1, \ldots, (m-1)$.
   (a) A value for $(\rho_{ss})_{i+1}$ is guessed.
   (b) All the variables on the RHS of the steady-state continuity equation (Eq. (12)) are now known. Using this equation, velocity $(u_{ss})_{i+1}$ is calculated. With a known velocity, Eqs. (13) and (14), are respectively solved for $(p_{ss})_{i+1}$ and $(h_{ss})_{i+1}$. Now, using this pressure and enthalpy values, state equation (15) is solved for density $(\tilde{\rho}_{ss})_{i+1}$. This step (i.e. step (b)) is repeated (until a desired convergence is reached) with this updated density value $(\tilde{\rho}_{ss})_{i+1}$ serving as a guess for $(\rho_{ss})_{i+1}$.

(4) At convergence, all of the unknown discrete variables are calculated, including a value for $(p_{ss})_m$.

(5) Calculated pressure at the outlet, $(p_{ss})_m$, is compared with the pressure p_{out} specified as the boundary condition. If the difference $|p_{out} - (p_{ss})_m|$ is within the specified tolerance limit, then the simulation terminates. Otherwise, step (3) is repeated with *another* guess value for $(u_{ss})_1$, until the pressure boundary condition at the exit (grid m) is satisfied within the specified tolerance. Improved guess for $(u_{ss})_1$ can be obtained by employing either the "Bisection method" or the "Regula-Falsi method". [Not surprisingly, Regula-Falsi method leads to faster convergence than the Bisection method.]

3.4.2. Solution algorithm for the time-dependent problem

The algorithm employed to solve the coupled, non-linear, time-dependent equations (Eqs. (18)–(21)) is given below (Chatoorgoon, 1986):

There are four unknown variables (ρ, u, p and h) to be solved at each time step for each grid point i.

I. *Initial condition*: at $t = 0$, all unknown variables are assumed to be known for each grid point i.
- $\rho_i^0 =$ known.
- $u_i^0 =$ known.
- $p_i^0 =$ known.
- $h_i^0 =$ known.

II. *Boundary conditions*: since inlet conditions of the flow channel are maintained constant, for each $(n+1)^{\mathrm{th}}$ time step ($n = 0, 1, 2, \ldots$), at grid point 1.
- $\rho_1^{n+1} = \rho_{in} =$ constant.
- $p_1^{n+1} = p_{in} =$ constant.
- $h_1^{n+1} = h_{in} =$ constant.

III. For the $(n+1)^{\mathrm{th}}$ time step,
   (a) Velocity at the channel inlet u_1^{n+1}, is guessed.
   (b) Following two steps ((b.1) and (b.2)) are repeated for $i = 1, \ldots, (m-1)$.
      (b.1) A value for ρ_{i+1}^{n+1} is guessed at the $(i+1)^{\mathrm{th}}$ grid point.
      (b.2) All the variables on the RHS of the time-dependent continuity equation (18) are now known. Using this equation, velocity u_{i+1}^{n+1} is calculated. With a known velocity, Eqs. (19) and (20), are respectively solved for p_{i+1}^{n+1} and h_{i+1}^{n+1}.

Now, using this pressure and enthalpy values, state equation (21) is solved for density $\tilde{\rho}_{i+1}^{n+1}$. This step (i.e. step (b.2)) is repeated (until a desired convergence is reached) with the updated density value $\tilde{\rho}_{i+1}^{n+1}$ serving as a guess for ρ_{i+1}^{n+1}.

(c) At convergence, all of the discrete unknown variables are calculated up to the outlet of the flow channel, including p_m^{n+1}.

(d) Calculated pressure at the outlet, p_m^{n+1}, is compared with the specified pressure boundary condition, p_{out}. If the difference $|p_{\text{out}} - p_m^{n+1}|$ is within the specified tolerance limit, then simulation moves to the next time step level. Otherwise, step IIIb is repeated with *another* guess value for u_1^{n+1} until the pressure boundary condition at the exit (grid m) is satisfied within the specified tolerance. Improved guess for u_1^{n+1} can be obtained by employing either the "Bisection method" or the "Regula-Falsi method".

A computer code called *f*low *i*nstability *a*nalysis under *s*uper*c*ritical *o*perating conditions (FIASCO) is written in FORTRAN90 to simulate the dynamics of a natural circulation loop with supercritical fluid using the algorithm discussed above. As a validation and verification exercise as well as to gain some insight into the natural circulation heat removal mechanism under supercritical conditions, several results available in literature (Lomperski et al., 2004; Jain, 2005) were first reproduced using this code. Simulated loop geometry along with the other system parameters are described in the following section.

4. Loop details

Steady-state and time domain analyses are carried out for a simple single-channel rectangular loop with supercritical carbon dioxide as the working fluid (same as in Chatoorgoon et al., 2005b; Voodi, 2004). CO_2 is often used in supercritical fluid experiments due to its viability and similarity in thermo-physical properties' variations compared to water at supercritical conditions. Moreover, due to lower critical pressure for CO_2, safety and power demands to conduct experiments are less taxing.

A schematic diagram and geometric parameters for the loop are shown in Fig. 2. It is a constant area loop with lower horizontal heating and upper horizontal cooling sections. Heat source and sink are assumed to be of equal magnitude, and uniformly distributed along the respective sections. Also, energy is assumed to be directly deposited to or extracted from the respective sections eliminating the need to model wall heat transfer mechanism. Both, inlet and outlet of the loop are assumed to be connected to a large reservoir or pressurizer chamber in order to maintain constant inlet conditions (i.e. constant pressure and temperature at point A). Also, a zero total pressure drop boundary condition is applied in the flow loop, which in turn provides another boundary condition at the exit (point O).

Reservoir temperature and pressure are maintained at 25 °C and 8 MPa, which provide inlet temperature, inlet pressure, and outlet pressure boundary conditions for the flow loop. Moreover, inlet and exit restriction loss coefficients – $R_{k_1} = 0.5$ and $R_{k_2} = 0.5$, respectively – are included, by modifying C_k as, $C_{k_i} = (f_i/2D_h) + (R_{k_i}/\Delta z)$ for the inlet and outlet grid points.

5. Steady-state analysis

For given parameter values, the steady-state solution is determined by solving the steady-state governing equations for the one-dimensional flow channel using the solution algorithm described in Section 3.4.1. The NIST REFPROP7 package (Lemmon et al., 2002) is modified and linked to the FORTRAN code. It is used as the state equation to provide thermo-physical properties data for CO_2. Steady-state behavior is simulated at different power levels while maintaining the inlet condition constant. The results in Fig. 3(a), obtained with a grid size of $\Delta x = 0.1$ m, show that the steady-state flow rate initially increases with power, reaches a maximum at about 2 MW and then decreases. While comparing steady-state results obtained using the FIASCO code with those obtained using the SPORTS code (shown in Fig. 3(b)), it is observed that the two flow-power curves match fairly well for low values of power. However, there exists some discrepancy in the after-peak region. A mesh sensitivity study is performed to assess the effects of spatial grid size on the steady-state flow-power curve, and is shown in Fig. 4. It is observed that results do change slightly with mesh refinement; however, the effect is insignificant. Therefore, spatial grid size of 0.1 m was chosen in subsequent steady-state and transient simulations.

6. Stability analysis

For the transient simulations, a slightly perturbed form of the steady-state solution for the unknown variables (ρ, u, p and h)

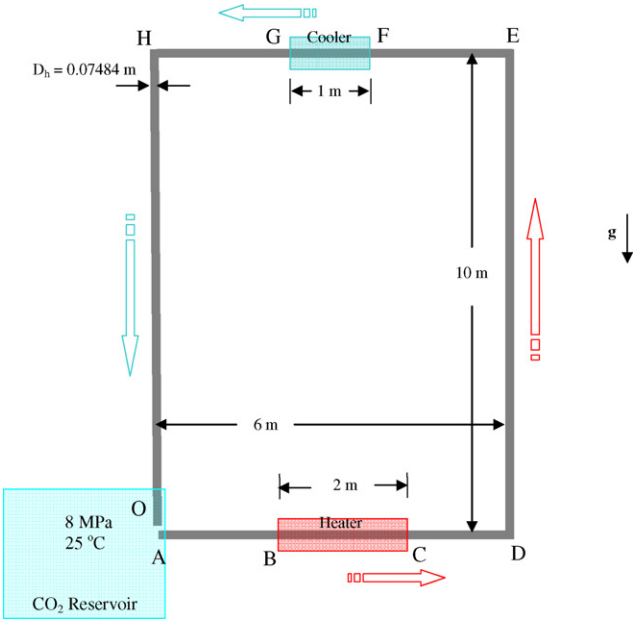

Fig. 2. Schematic diagram of the flow loop.

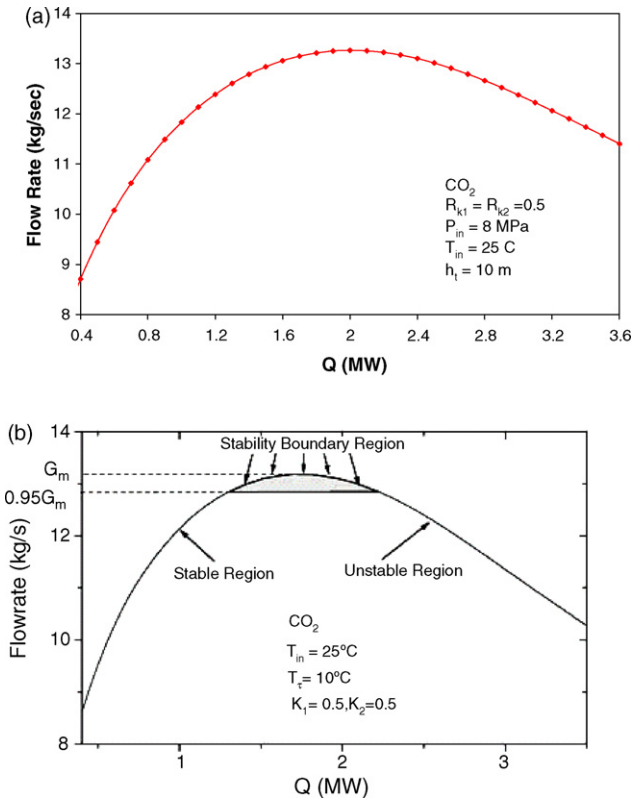

Fig. 3. Steady-state flow rate profile for CO_2 (with 0.1 m grid size): (a) FIASCO and (b) Chatoorgoon et al. (2005b).

is used as an initial condition at every grid point. Perturbations can be introduced in any of the unknown variables. Only velocities were perturbed in the analysis presented here. Steady-state velocities are perturbed (increased) by 1% and used as initial condition. Starting with this initial condition, discrete variables at every time step are evaluated throughout the domain using the algorithm given in Section 3.4.2 with the exit pressure boundary condition satisfied within the tolerance limit of 10^{-6} MPa. If, the perturbation grows in time, i.e. oscillations in inlet velocity (and velocity at all grid points) diverge as time increases, then the system is considered to be unstable. Otherwise, if the perturbation decays in time, i.e. inlet velocity oscillations dampen and

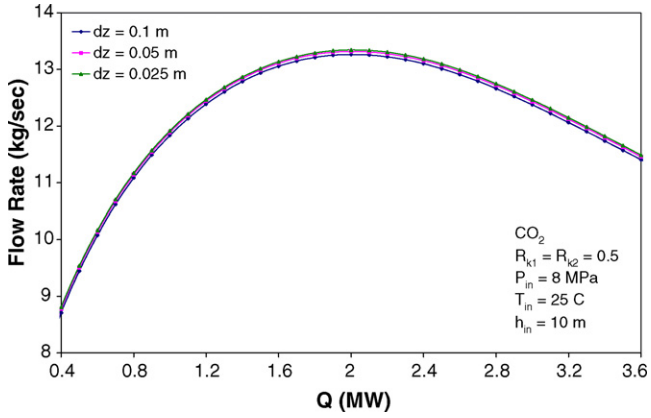

Fig. 4. Effect of spatial mesh refinement on the steady-state results.

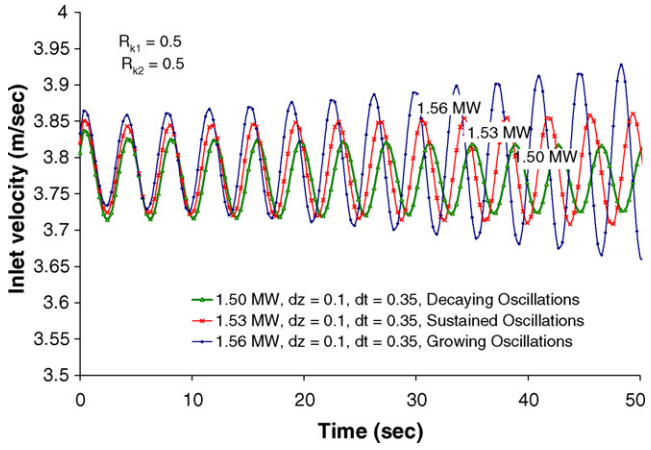

Fig. 5. Inlet velocity as a function of time for three different power levels. The stability boundary is between 1.50 MW and 1.53 MW (with $\Delta z = 0.1$ m and $\Delta t = 0.35$ s).

inlet velocity returns to its steady-state value, then the system is considered to be stable. Power level at which flow oscillations nearly sustain their amplitude (i.e. neither diverge nor converge), is called the threshold power (stability boundary) for that flow system.

The initial round of transient analyses with the FIASCO code is carried out with a spatial grid size of 0.1 m and time step size of 0.35 s (same as in Chatoorgoon et al., 2005b). Flow corresponding to a finite number of steady-state solutions on the power-flow curve is perturbed and the growth or decay of perturbation over time, which indicates whether the system at this steady state is unstable or stable, is monitored. Inlet velocity evolution for two different power levels is shown in Fig. 5. From the results shown in Fig. 5, it is clear that the flow oscillations with power at 1.50 MW decay, i.e. the system at this power level is stable. Flow oscillations with power at 1.53 MW grow, i.e. the system is unstable, and hence the power threshold for stability for this system is between $1.50 < P < 1.53$ MW. This is in good agreement with the results reported in Chatoorgoon et al. (2005b) *for the same spatial grid size and time step* and shown in Fig. 3(b).

6.1. *Effect of numerical discretization parameters*

In an attempt to reproduce the results reported by previous investigators, results presented in Fig. 5 were obtained with $\Delta z = 0.1$ m and $\Delta t = 0.35$ s. However, to ensure temporal and spatial grid independence of the results, a grid refinement study is performed and the results, presented in the subsections below, show that the stability threshold does in fact change as spatial and temporal steps are refined.

6.1.1. *Effect of temporal grid refinement*

For the temporal grid refinement study, a power level of 1 MW, which is well below the stability threshold value of ~1.515 MW, is chosen, and the system is found to be highly stable for the spatial grid size of 0.1 m and the time step size of 0.35 s. As shown in Fig. 6, further reducing the time step by half and quarter values, while keeping the spatial grid size at 0.1 m, produces sustained and growing flow oscillations, respectively,

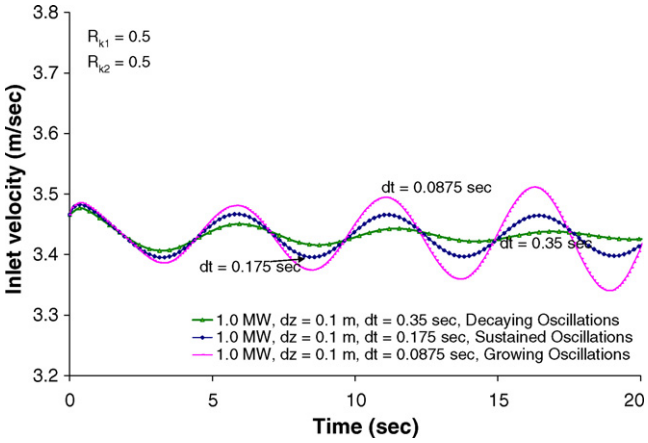

Fig. 6. Effect of reducing time step on the transient solution at 1.0 MW.

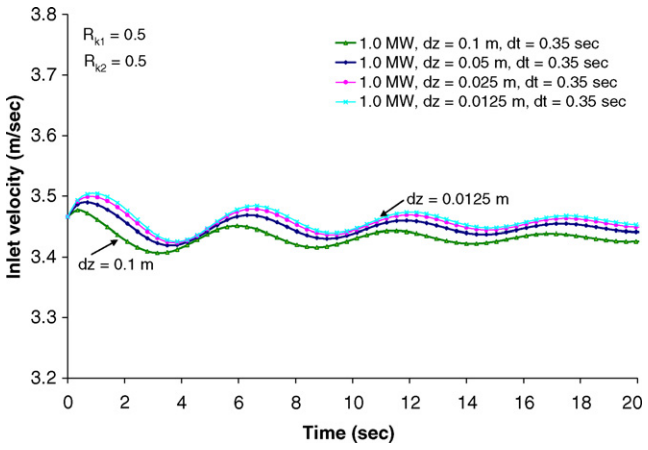

Fig. 8. Effect of reducing spatial grid size on the transient solution at 1.0 MW.

suggesting that $\Delta t = 0.35$ s is too large a time step for accurate stability analysis. It is well known that a large time step may induce numerical diffusion and hence (artificial) flow stability into the system. Further reductions of the time step yield the time step size independent converged solution at $\Delta t = 0.021875$ (0.35/16) s, as shown in Fig. 7.

It should be noted that though temporal grid refinement steps are not reported by Jain (2005), results presented in that reference are obtained with time steps closer to 0.02 s.

6.1.2. *Effect of spatial grid refinement*

To ensure the convergence of the numerical solution, a spatial grid refinement study is also performed. Effects of different grid size on the numerical solution are shown in Figs. 8 and 9 for 1.0 MW and 0.7 MW power, respectively.

In Fig. 8, temporal variation in inlet velocity is presented for different spatial grid sizes at a power level of 1.0 MW. Note that the time step used for results in this figure is 0.35 s. [Though the system is seen to be stable for this time step (as shown in Fig. 8), the system is actually unstable at smaller time step values.] It can be seen that reducing the spatial grid size does not have a significant effect on system stability, as the system remains stable at finer spatial resolutions producing spatially converged results. Though a shift in oscillations is observed, the magnitude and frequency of oscillations remain nearly the same.

Furthermore, to predict the effect of spatial grid resolution on an *actually* stable system, a grid refinement study is performed at a power level of 0.7 MW and results obtained using $\Delta t = 0.02$ s are shown in Fig. 9. Once again, it is clear that a nearly stable system remains so as Δz is refined, suggesting that $\Delta z = 0.1$ m is adequate for the stability analysis of this system.

6.1.3. *Effect of tolerance permitted in imposition of pressure boundary condition*

In order to accurately predict the stability threshold of the system, it is noted that the pressure boundary condition at the outlet of the channel should be strictly satisfied. Otherwise, the results could be misleading. The effect of tolerance level permitted in the imposition of pressure boundary conditions at the exit (parameter *pb*) on the numerical evaluation of system stability is shown in Fig. 10. It is clear that an unstable system can be predicted to be stable if the tolerance is too large. By numerical experiments it is determined that a tolerance equal to 10^{-6} MPa or less in the pressure boundary condition yields a converged solution, and should be used in the numerical simulations.

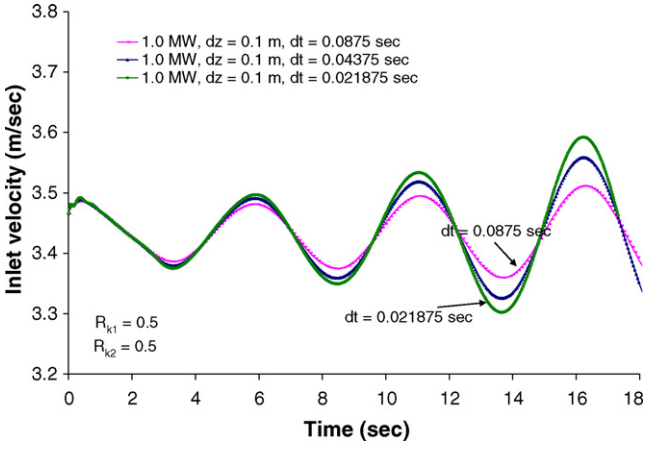

Fig. 7. Further time step refinement at 1.0 MW.

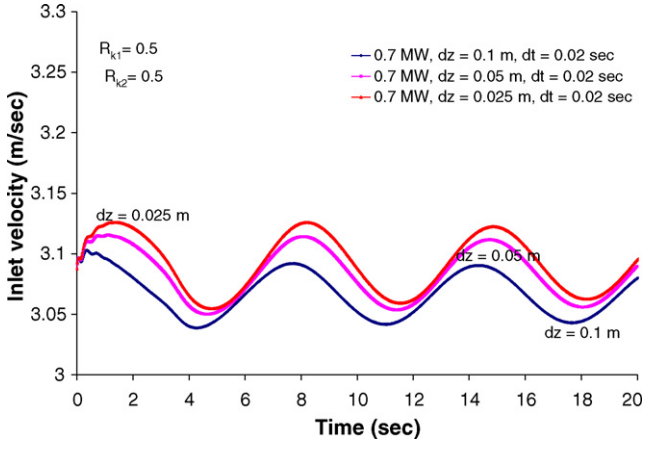

Fig. 9. Effect of reducing spatial grid size on the transient solution at 0.7 MW.

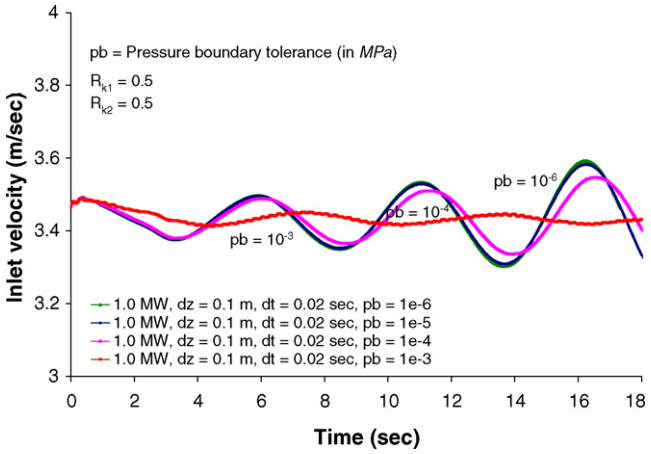

Fig. 10. Effect of tolerance permitted in imposition of pressure boundary condition at 1.0 MW.

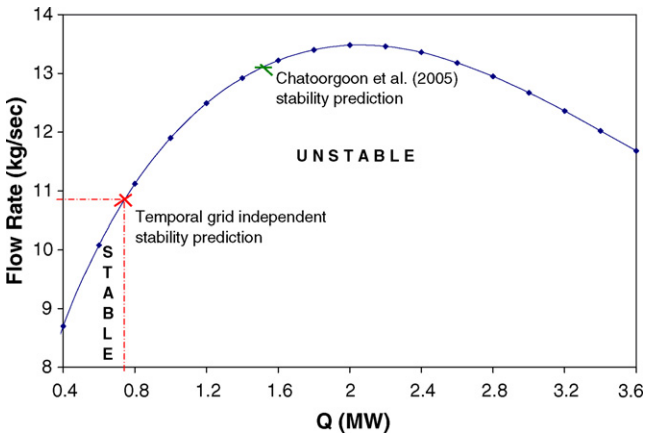

Fig. 12. Comparison of stability prediction with previous investigations.

6.2. Stability threshold

To locate the stability threshold on the steady-state flow-power curve, applied power is incremented in small steps, and the time-dependent set of conservation equations are numerically solved with the temporal and spatial grid size of 0.02 s and 0.1 m, respectively. Minimum power level at which sustained or growing oscillations are obtained is the stability threshold. Spatial grid size was retained as 0.1 m to predict the stability limit as reducing it further did not show any effect on stability, although a phase shift in oscillations is observed. The tolerance for the exit pressure boundary condition is set at 10^{-6} MPa. Specifically, transient solutions for 0.70 MW and 0.80 MW lead to stable and unstable flow oscillations, respectively. Results are shown in Fig. 11. The stability threshold is hence found to be near 0.75 MW. A comparison with previous investigations is shown in Fig. 12.

6.3. Parametric effects on stability

The stability characteristics of the CO_2 natural circulation loop are studied using the FIASCO code. The system is analyzed for different operating conditions and geometric parameters to evaluate their influence on stability.

6.3.1. Effect of pressure

For the CO_2 natural circulation loop under supercritical conditions, an increase in system pressure (while keeping other system parameters constant) is found to have a stabilizing effect. Fig. 13 shows the stability threshold on the flow-power curve for two pressure levels. Changing the system pressure from 8 MPa to 10 MPa increased the threshold power by 0.20–0.95 MW. Such stabilizing effects of increasing pressure on flow stability are well known for two-phase natural circulation loops. In two-phase natural circulation loops, for a given input power, increasing system pressure reduces the void fraction and that, in turn, decreases the two-phase flow friction and momentum pressure drops and, thus, stabilizes the system (Boure et al., 1973).

6.3.2. Effect of inlet subcooling

Similar to increasing system pressure, an increase in inlet degree of subcooling from 6 °C to 16 °C leads towards 0.05 MW increase in threshold power and thus stabilizes the flow system, as shown in Fig. 14. Here, degree of subcooling is defined with reference to the critical temperature of CO_2 (31 °C). Unlike the

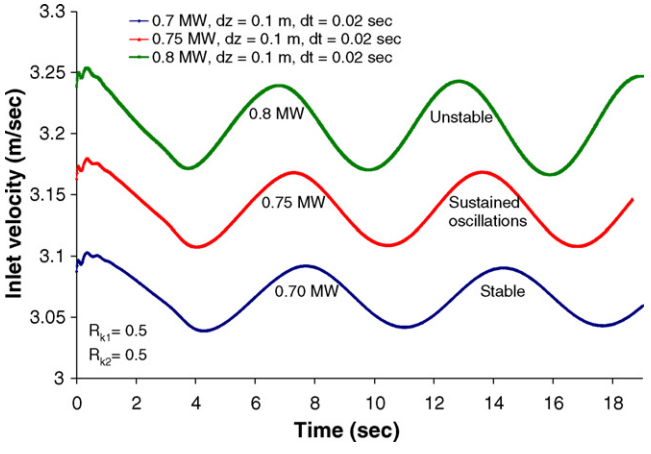

Fig. 11. Transient solution for three power levels.

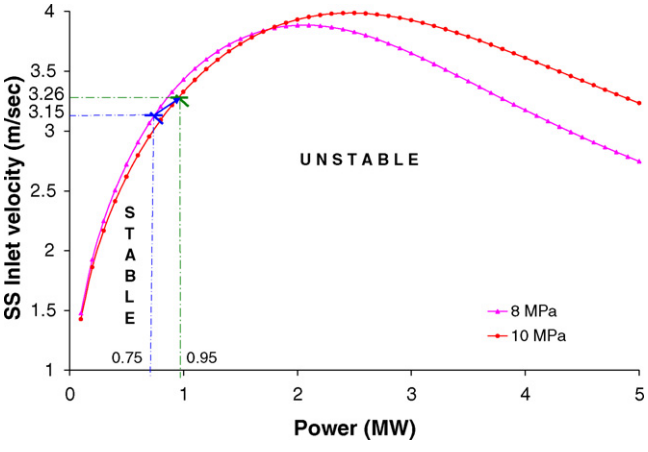

Fig. 13. Effect of pressure on the stability threshold.

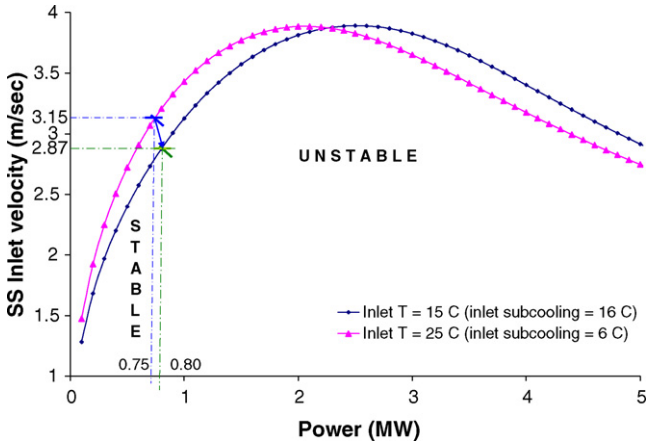

Fig. 14. Effect of inlet subcooling on the stability threshold.

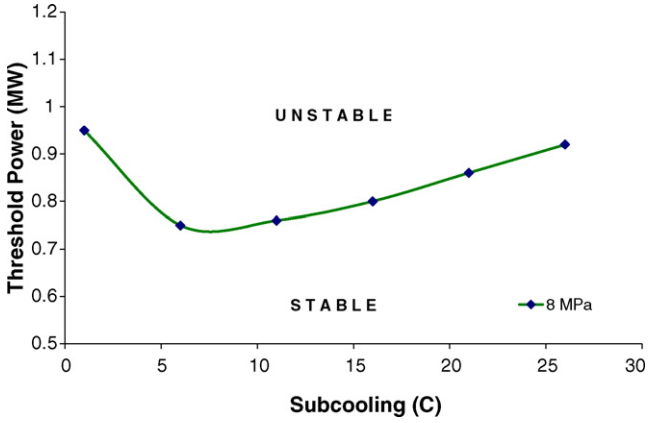

Fig. 15. Effect of inlet subcooling on threshold power.

case with pressure increase which leads to a higher flow rate at the new threshold power, an increase in degree of subcooling leads to a lower flow rate at the new stability threshold.

Fig. 15 shows the stability threshold plotted in the power-subcooling plane. It is observed that the effect of inlet subcooling on flow stability exhibits a minimum. For small subcoolings, increasing inlet subcooling destabilizes the flow, whereas for high subcooling the effect is stabilizing. Similar behavior is observed in various two-phase heated channel systems, where an increase in inlet subcooling from medium or high levels results in larger non-boiling length and reduced void fraction and, thus, stabilizes the flow system. However, an increase in inlet subcooling from a small value destabilizes the flow due to significant incremental change of transit time (Boure et al., 1973).

7. Discussion and conclusions

Results obtained for the stability threshold using the FIASCO code deviate substantially from the results reported in Chatoorgoon et al. (2005b) (see Fig. 12). These results are in disagreement with the findings reported in Chatoorgoon et al. (2005b) that showed the stability threshold to be *near-the-peak* (Chatoorgoon et al., 2005b), as shown in Fig. 3(b). The disagreement in results is most likely due to the undesirable dissipative and dispersive effects induced by the large time steps used in reported studies, thereby leading to a larger stable region than those found using smaller time steps. This high sensitivity of numerical scheme on the time step size has recently been verified in Chatoorgoon et al. (2007), where they carried out a time step refinement study and found that a time step of 0.05 s was necessary in order to yield temporally converged solutions. Results presented here are also supported by the linear stability analysis of the natural circulation loop, reported in Jain (2005), where it was also concluded that the stability threshold is not strictly restricted to the peak region of the steady-state flow-power curve. Thus, it can be concluded that the stability threshold of a natural circulation loop with supercritical fluid, is not confined to the *near-peak region* of the (steady state) flow-power curve. Results obtained for the range of parameter values used in this investigation always predict the threshold power to be in the positive slope region of the (steady state) flow-power curve. However, due to lack of experimental studies with supercritical fluids in a natural circulation loop, presently there are not enough experimental data available to benchmark numerical findings. Therefore, more experimental studies should be carried out to verify the numerical predictions. Parametric studies for different operating conditions reveal the similarity of stability characteristics under supercritical conditions with those in two-phase flows.

References

Ambrosini, W., Sharabi, M.B., 2006. Dimensionless parameters in stability analysis of heated channels with fluids at supercritical pressure. In: Proceedings of ICONE-14, Miami, FL, USA, July 17–20, 2006 (Paper 89862).

Boure, J.A., Bergles, A.E., Tong, L.S., 1973. Review of two-phase instability. Nucl. Eng. Des. 25, 165–192.

Buongiorno, J., 2004. The supercritical water cooled reactor: ongoing research and development in the U.S. In: Proceedings of ICAPP'04, Pittsburgh, PA, USA, June 13–17, 2004 (Paper 4229).

Chatoorgoon, V., 1986. A simple thermalhydraulic stability code. Nucl. Eng. Des. 93, 51–67.

Chatoorgoon, V., 2001. Stability of supercritical fluid flow in a single-channel natural-convection loop. Int. J. Heat Mass Transfer 44, 1963–1972.

Chatoorgoon, V., Upadhye, P., 2005. Analytical studies of supercritical flow instability in natural convection loops. In: Proceedings of the 11th International Topical Meeting on Nuclear Reactor Thermal-Hydraulics (NURETH-11), Avignon, France, October 2–6 (Paper 165).

Chatoorgoon, V., Voodi, A., Fraser, D., 2005a. The stability boundary for supercritical flow in natural convection loops. Part I. H_2O studies. Nucl. Eng. Des. 235 (24), 2570–2580.

Chatoorgoon, V., Voodi, A., Upadhye, P., 2005b. The stability boundary for supercritical flow in natural convection loops. Part II. CO_2 and H_2. Nucl. Eng. Des. 235 (24), 2581–2593.

Chatoorgoon, V., Shah, M., Duffey, R., 2007. Linear predictions of supercritical flow instability in parallel channels. In: Proceedings of 3rd International Symposium on SCWR-Design and Technology, Shanghai, China, March 12–15, 2007 (Paper SCR2007-P009).

Generation IV International Forum (GIF), 2002. A technology roadmap for the Generation IV nuclear energy systems. GIF-002-00.

Gomez, O.T., Class, A., Lahey Jr., R.T., Schulenburg, T., 2006. Stability analysis of a uniformly heated channel with supercritical water. In: Proceedings of ICONE-14, Miami, FL USA, July 17–20, 2006 (Paper 89733).

Harvey, A.H., Peskin, A.P., Klien, S.A., 2004. NIST/ASME Steam Properties, Version 2.21. US Department of Commerce, Technology Administration, National Institute of Standards and Technology.

Jain, R., 2005. Thermal-hydraulic instabilities in natural circulation flow loops under supercritical conditions. Ph.D. Thesis, University of Wisconsin Madison, USA.

Jain, P., Rizwan-uddin, 2006. Steady state and dynamic analyses of supercritical CO_2 natural circulation loop. In: Proceedings of ICONE-14, Miami, FL, USA, July 17–20, 2006 (Paper 89103).

Lemmon, E.W., McLinden, M.O., Huber, M.L., 2002. NIST Reference Fluid Thermodynamic and Transport Properties—REFPROP, Version 7.0. US Department of Commerce, Technology Administration, National Institute of Standards and Technology.

Lomperski, S., Cho, D., Jain, R., Corradini, M.L., 2004. Stability of a natural circulation loop with a fluid heated through the thermodynamic pseudocritical point. In: Proceedings of ICAPP'04, Pittsburgh, PA, USA, June 13–17 (Paper 4268).

McAdams, W.H., 1954. Heat Transmission, third ed. McGraw-Hill, New York.

Pioro, I.L., Khartabil, H.F., Duffey, R.B., 2004. Heat transfer to supercritical fluids flowing in channels—empirical correlations (survey). Nucl. Eng. Des. 230, 69–91.

Voodi, V.A., 2004. Analytical study of non-dimensional parameters governing supercritical flow instabilities. M.Sc. Thesis, University of Manitoba, Canada.

Yamaji, A., Oka, Y., Koshizuka, S., 2005. Three-dimensional core design of high temperature supercritical-pressure light water reactor with neutronic and thermal-hydraulic coupling. J. Nucl. Sci. Technol. 42 (1), 8–19.

Yang, W.S., Zavaljevski, N., 2003. Preliminary investigation of power-flow instabilities of supercritical water reactor. ANL, Technical Report.

Yang, W.S., Zavaljevski, N., 2004. Effect of water rods and heat transfer correlations on SCWR stability. ANL, Technical Report.

Zappoli, B., 2003. Near-critical fluid hydrodynamics. C. R. Mecanique 331, 713–726.